Commun. Comput. Phys.
doi: 10.4208/cicp.070513.220713a

Vol. **15**, No. 3, pp. 596-617
March 2014

Chaotic Lid-Driven Square Cavity Flows at Extreme Reynolds Numbers

Salvador Garcia*

Instituto de Ciencias Físicas y Matemáticas, Universidad Austral de Chile, Casilla 567, Valdivia, Chile.

Received 7 May 2013; Accepted (in revised version) 22 July 2013

Communicated by Roger Temam

Available online 18 October 2013

Abstract. This paper investigates the chaotic lid-driven square cavity flows at extreme Reynolds numbers. Several observations have been made from this study. Firstly, at extreme Reynolds numbers two principles add at the genesis of tiny, loose counterclockwise- or clockwise-rotating eddies. One concerns the arousing of them owing to the influence of the clockwise- or counterclockwise currents nearby; the other, the arousing of counterclockwise-rotating eddies near attached to the moving (lid) top wall which moves from left to right. Secondly, unexpectedly, the kinetic energy soon reaches the qualitative temporal limit's pace, fluctuating briskly, randomly inside the total kinetic energy range, fluctuations which concentrate on two distinct fragments: one on its upper side, the upper fragment, the other on its lower side, the lower fragment, switching briskly, randomly from each other; and further on many small fragments arousing randomly within both, switching briskly, randomly from one another. As the Reynolds number $\mathrm{Re}\to\infty$, both distance and then close, and the kinetic energy fluctuates shorter and shorter at the upper fragment and longer and longer at the lower fragment, displaying tall high spikes which enlarge and then disappear. As the time $t\to\infty$ (at the Reynolds number Re fixed) they recur from time to time with roughly the same amplitude. For the most part, at the upper fragment the leading eddy rotates clockwise, and at the lower fragment, in stark contrast, it rotates counterclockwise. At $\mathrm{Re}=10^9$ the leading eddy — at its qualitative temporal limit's pace — appears to rotate solely counterclockwise.

AMS subject classifications: 76D99, 35Q30, 37N10
Key words: Navier-Stokes equations, lid-driven square cavity flows, chaos.

1 Introduction

As the Reynolds number $\mathrm{Re}\to\infty$ the temporal limit [13, p. 659] (at the Reynolds number Re fixed and as the time $t\to\infty$) of the lid-driven square cavity flow evolves from station-

*Corresponding author. *Email address:* sgarcia@uach.cl (S. Garcia)

ary to periodic and then to aperiodic, which means simply that it has definitely lost but still resembles somewhat periodicity. Yet afterwards, it definitely looses aperiodicity and becomes chaotic.

Specifically, for $\mathrm{Re} \leq 7{,}307.75$, it is stationary; for $7{,}308 \leq \mathrm{Re} \leq 13{,}393.5$, periodic; for $13{,}393.75 \leq \mathrm{Re} \leq 200{,}000$, aperiodic. Yet afterwards, at $\mathrm{Re} = 500{,}000$, it is chaotic. So it switches from stationary to periodic somewhere between $\mathrm{Re} = 7{,}307.75$ and $\mathrm{Re} = 7{,}308$; from periodic to aperiodic, somewhere between $\mathrm{Re} = 13{,}393.5$ and $\mathrm{Re} = 13{,}393.75$ [26]; from aperiodic to chaotic, somewhere between $\mathrm{Re} = 200{,}000$ and $\mathrm{Re} = 500{,}000$ [27].

Throughout, the moving (lid) top wall moves from left to right. And until $\mathrm{Re}=200{,}000$ the leading eddy rotates solely clockwise. But at $\mathrm{Re} = 500{,}000$ it rotates sometimes clockwise and at other times counterclockwise, mostly equally, a competition for becoming the leading eddy taking place before switching from each other [27].

A combination of known methods [25] is used to discretize and solve the Navier-Stokes equations: the linear Linθ^*-scheme [44] (a variant of the nonlinear θ-scheme [30], [23, p. 460]), an orthogonal projection algorithm [38], the Conjugate Gradient method [12], the Bi-CGSTAB method [50], the Fast Fourier Transform method [18,47,48], SuperLU [14] — and the incremental unknowns method [4–11, 19–28, 31, 37, 45, 46, 49] as a spatial preconditioner. The linear Linθ^*-scheme is used for the temporal discretization — Δt is the time step — and a staggered marker-and-cell (MAC) mesh with finite-differences [32] is used for the spatial discretization — $h = 1/256 = 0.00390625$ is the spatial mesh size. At each temporal iteration two generalized Stokes equations and two linear elliptic equations with variable coefficients must be solved.

Yet, how the temporal limit behaves for extreme Reynolds numbers — has it been definitely reached — and what is the time needed to reach it?

To gain insight on these questions, let us consider the extreme cases $\mathrm{Re} = 10^6$, 10^8, $5 \cdot 10^8$, 10^9. As before [26, 27], a Direct Numerical Simulation (DNS) which runs from $t = 0$ to a sufficiently long time t_∞ simulates the flow, and then direct observations of it for the most part past the time t_∞ are at the core of the temporal limit's study. At $\mathrm{Re} = 10^6$ as at $\mathrm{Re}=500{,}000$ the time step $\Delta t = 2h = 0.0078125$ and $t_\infty = 150{,}000$, a DNS involving a total of 19,200,000 temporal iterations. But at $\mathrm{Re}=10^8$, $5 \cdot 10^8$, 10^9 the time step must be reduced to $\Delta t = h = 0.00390625$, and then because of computational costs, t_∞ is reduced sometimes to $t_\infty = 50{,}000$, a DNS involving a total of 12,800,000 temporal iterations. At each Reynolds number two DNS are conducted: (1) fluid starting from data and (2) fluid starting from rest. For fluid starting from data the initial condition is the numerical solution computed at some time at a prior Reynolds number.

At extreme Reynolds numbers the flow is difficult to study mainly for two reasons. First, for the leading eddy to switch from rotating counterclockwise to clockwise, the DNS ought to run for a sufficiently long time interval, the switching occurring somewhere in between. But to determine what triggers the switching, it must be restarted shortly before the switching and therefore run for a short time interval, highly likely missing the switching. Second, all the restartings coincide at the beginning for a short while, then progressively differ for a short while — and afterwards significantly differ,

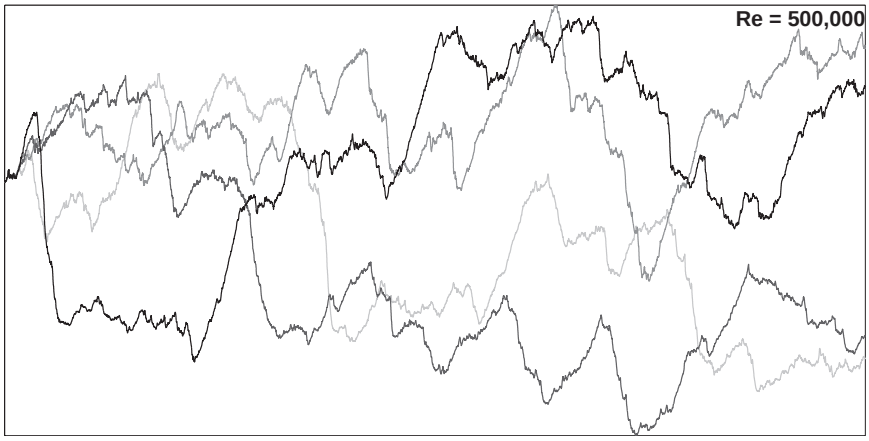

Figure 1: Kinetic energy from $t=146{,}093.75$ to $t_\infty=150{,}000$.

making hard to retrieve any former simulation. At $\mathrm{Re}=500{,}000$ see Fig. 1 for several restartings from $t=146{,}093.75$ to $t_\infty=150{,}000$, each involving a total of 500,000 temporal iterations; they coincide roughly from $t=146{,}093.75$ to $t=146{,}117.25$, each involving a total of 3,000 temporal iterations.

Notwithstanding, the DNS's allow to understand distinctive features of the flow.

In the first place, at extreme Reynolds numbers two principles add at the genesis of tiny, loose counterclockwise- or clockwise-rotating eddies (cf. [27, p. 1741]):

Third principle The currents nearby within a clockwise- or counterclockwise-rotating eddy eventually may create a bend which may then influence the globally clockwise- or counterclockwise-rotating fluid inside the bend to whirl locally counterclockwise or clockwise, a whirling which may further arouse deeper inside the bend a tiny, loose counterclockwise- or clockwise-rotating eddy.

Fourth principle A strong, still clockwise-rotating eddy attached to the moving (lid) top wall leaves it somewhere to turn away from it, arousing closely rightward, within itself, near attached to the moving (lid) top wall, a tiny, loose counterclockwise-rotating eddy — perhaps stirring this up.

Fig. 2 illustrates the third principle. The fluid surrounding the circle rotates clockwise (black streamlines). This includes two clockwise-rotating Bézier curves parts of two clockwise-rotating eddies surfacing within a widespread clockwise-rotating eddy and a clockwise-rotating bend created between both. Nevertheless, the currents nearby influence the fluid at and within the circle to whirl locally counterclockwise, giving rise to a tiny, loose counterclockwise-rotating eddy (light-gray streamline). This principle flashes out already at $\mathrm{Re}=30{,}000$ [26, p. 564].

Fig. 3, the fourth. A clockwise-rotating eddy attached to the moving (lid) top wall, a clockwise-rotating Bézier curve (black streamline) part of this, leaves it somewhere to

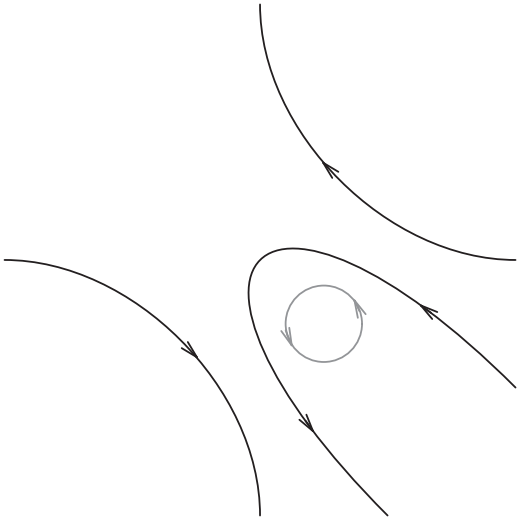

Figure 2: Streamlines for a Third principle's illustration.

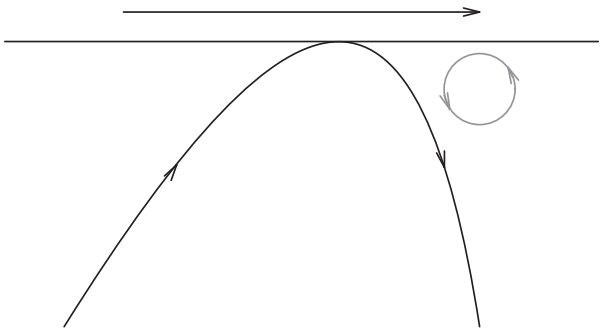

Figure 3: Streamlines for a Fourth principle's illustration.

turn away from it, arousing closely rightward, within itself, near attached to the moving (lid) top wall, a tiny, loose counterclockwise-rotating eddy (light-gray streamline). This principle resembles the First principle [27, p. 1741] but for a moving wall.

In the second place, unexpectedly, for fluid starting from data or from rest, from $t=0$ to $t=t_\infty$, the kinetic energy soon reaches the qualitative temporal limit's pace, fluctuating briskly, randomly inside the total kinetic energy range, fluctuations which concentrate on two distinct fragments: one on its upper side, the upper fragment, the other on its lower side, the lower fragment, switching briskly, randomly from each other; and further on many small fragments arousing randomly within both, switching briskly, randomly from one another.

When the kinetic energy's lines for fluid starting from rest and from data display together, a bold one means fluid starting from rest; a light one, fluid starting from data.

At Re$=$500,000 both fragments, scarcely its upper half and its lower half, barely over-

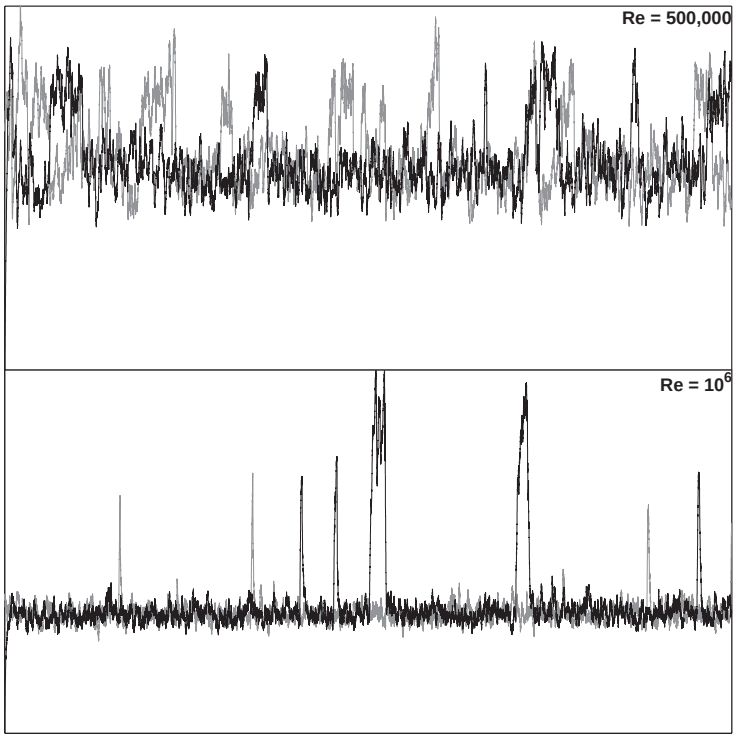

Figure 4: Kinetic energy from $t=0$ to $t_\infty=150{,}000$.

lap, and the kinetic energy remains mostly equally at both (see Fig. 4). As the Reynolds number $\mathrm{Re}\to\infty$, both distance and then close, and the kinetic energy fluctuates shorter and shorter at the upper fragment and longer and longer at the lower fragment, displaying tall high spikes which enlarge and then disappear. As the time $t\to\infty$ (at the Reynolds number Re fixed) they recur from time to time with roughly the same amplitude.

For the most part, at the upper fragment the leading eddy rotates clockwise, and at the lower fragment, in stark contrast, it rotates counterclockwise. For the kinetic energy to switch from the lower fragment to the upper fragment and conversely, it must then switch direction of rotation, switchings which occur from clockwise to counterclockwise at the lower side of the upper fragment and from counterclockwise to clockwise at the upper side of the lower fragment.

At $\mathrm{Re}=10^9$ the leading eddy — at its qualitative temporal limit's pace — appears to rotate solely counterclockwise.

Yet, are the chaotic temporal limits distorted by the inherent numerical errors arising from the use of a coarse spatial mesh size such as $h=1/256=0.00390625$ or a coarse time step such as $\Delta t=2h=0.0078125$ or $\Delta t=h=0.00390625$?

First of all, let us observe that the chaotic temporal limits are sensitive to the variations of the extreme Reynolds numbers, sensitivity detected by the variations of the tall high spikes displayed by the kinetic energy.

Second, the effect of the spatial-mesh-size or time-step refining has been assessed for stationary and periodic temporal limits [26]. Roughly, the conclusion is that the inherent numerical errors arising from the use of a coarse spatial mesh size or a coarse time step add to the Reynolds number. That is, the solution computed at a Reynolds number with a coarse mesh size or a coarse time step predicts the one computed at a greater Reynolds number with a finer mesh size or a finer time step. These computational experiments hint at the persistence of the chaotic temporal limit's qualitative behavior throughout the spatial-mesh-size or time-step refining, computational experiments out of reach, however, for chaotic temporal limits because of computational costs.

Finally, it is not certain that the flow described actually represents the flow at the Reynolds numbers $\mathrm{Re}=10^6$, 10^8, $5\cdot10^8$, 10^9, but still appears an interesting dynamic totally different from the dynamic observed [25–27] at Reynolds numbers consistent with the spatial mesh size $\left(\mathrm{Re}=\mathcal{O}(\frac{1}{h^2})\right)$.

The lid-driven square cavity flow — an almost fictitious flow [42] — has already been solved many times at many Reynolds numbers by many techniques [1–3,16,17,23,25–27, 29,31,34,35,39,51], yet DNS's at extreme Reynolds numbers appear scarce [4] — if not absent.

This article is organized as follows. Section 2 deals with flows at extreme Reynolds numbers: $\mathrm{Re}=10^6$, 10^8, $5\cdot10^8$, 10^9. And Section 3 summarizes the main points.

2 Flows at extreme Reynolds numbers

First, let us consider the case $\mathrm{Re}=10^6$; and then, together, the cases $\mathrm{Re}=10^8$, $5\cdot10^8$, 10^9.

2.1 The case $\mathrm{Re}=10^6$

At $\mathrm{Re}=10^6$, for fluid starting from data and from rest, from $t=0$ to $t_\infty=150{,}000$, the kinetic energy's behavior resembles somewhat the corresponding one at $\mathrm{Re}=500{,}000$ (see Fig. 4).

The differences. The lower fragment and the upper fragment distance: the lower fragment settles down at the bottom; the upper fragment, up at the top. The kinetic energy switches briskly, randomly from each other, and fluctuates less at the upper fragment and more at the lower fragment, displaying tall high spikes which recur from time to time.

The similarities. For fluid starting from data and from rest, qualitatively the kinetic energy soon fluctuates similarly.

Next, let us see how the kinetic energy's fluctuations relate to the leading eddy's switching direction of rotation.

The kinetic energy increasing towards a tall high spike at the upper fragment, the leading eddy — a widespread eddy attached somewhat to all walls — rotates clockwise.

Wide counterclockwise-rotating eddies loop clockwise. After a while, one stays put for a while at the top right corner. And then, one standing out at the top left corner catches this up. Afterwards, one merges downwards and leftwards with the amalgam,

forming out a widespread counterclockwise-rotating amalgam stretching out from the left wall's downside to the left wall's upside and from there to the right wall's upside. It is attached to the left wall nearly two-thirds and to the right wall somewhat a little bit below the top right corner. Surrounding it downwards, stands out a strong clockwise-rotating eddy which stretches out from most of the bottom wall to part of the left wall and to a great extent of the right wall, filling out nearly one-half of the square cavity. As a whole, it moves upwards and leftwards, detaches from the right wall, and then moves further upwards, diminishes, and again attaches to the right wall. Yet, it is caught up upwards the bottom left corner by one which has stood out for a while at the bottom left corner, forming out again a widespread counterclockwise-rotating amalgam stretching out from the bottom left corner to the top left corner and from there to the top right corner. Surrounding it downwards and rightwards, stands out a clockwise-rotating eddy, strong, attached to the bottom wall and to the right wall filling out a little bit more than one-fourth of the square cavity: the leading eddy — staying put.

The widespread counterclockwise-rotating amalgam widens further. Just before the kinetic energy reaches the top of the tall high spike, it becomes — for an instant — the leading eddy. The former leading eddy, clockwise-rotating, moves upwards, detaching it from the right wall. And then it diminishes. When the kinetic energy is at the top of the tall high spike, the leading eddy rotates clockwise again and continues so, the kinetic energy diminishing towards a low spike at the downside of the upper fragment. Meanwhile, it merges and splits everywhere. Just before the kinetic energy reaches the bottom of the low spike, it attains its maximum. When the kinetic energy is at the bottom of the low spike, the leading eddy rotates counterclockwise. And then the kinetic energy remains at the downside of the upper fragment, fluctuating briskly, randomly, the leading eddy rotating alternatively counterclockwise or clockwise for a while.

For the most part, at the lower fragment the leading eddy rotates counterclockwise.

Next, let us see occurrences of the Third and Fourth principles.

In the first place, a bend may occur at the border of dissimilarly rotating eddies, between two or several similarly rotating eddies, in the wake of a counterclockwise- or clockwise-rotating eddy looping clockwise or counterclockwise, providing occurrences of the Third principle. Five instances display below.

First, a bend at the border of dissimilarly rotating eddies at the bottom left corner (see Fig. 5). A small counterclockwise-rotating eddy and another to its right, both attached to the bottom wall a little bit to the right of the bottom left corner, glide towards the bottom left corner. The latter merges with the former as this reaches the bottom left corner, forming out a small counterclockwise-rotating amalgam at the bottom left corner which arouses a tiny clockwise-rotating eddy exactly at the bottom left corner. A wide counterclockwise-rotating eddy looping clockwise reaches the bottom left corner, merges with the amalgam, and then merges with a small counterclockwise-rotating eddy attached to the left wall a little bit below the center of the left wall, enclosing just below this a small clockwise-rotating eddy attached to the left wall which detaches from the left wall and — dwindling — loops counterclockwise within it, its remnant soon vanish-

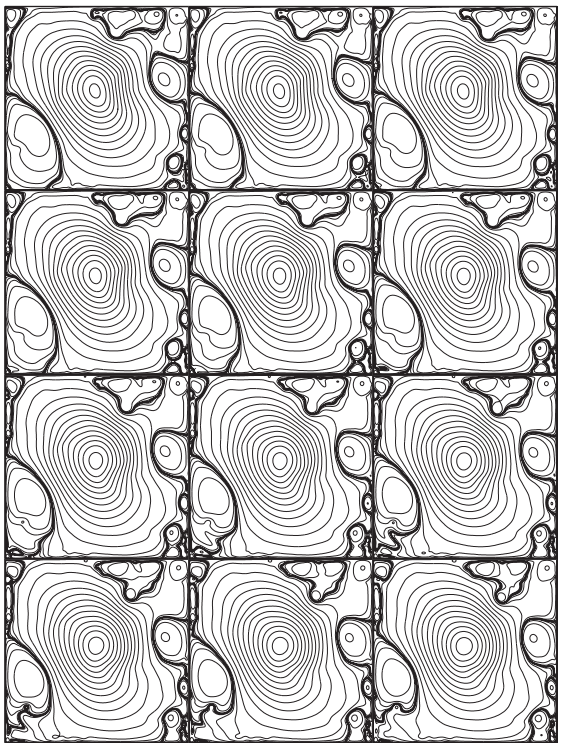

Figure 5: A Third principle's occurrence at the bottom left corner. $\mathrm{Re}=10^6$.

ing. While moving upwards, it arouses a tiny clockwise-rotating eddy attached to the left wall a little bit above the bottom left corner. The tiny clockwise-rotating eddy exactly at the bottom left corner and this merge along the left wall, and then the amalgam grows further upwards along the left wall. Reaching the tiny clockwise-rotating eddy exactly at the bottom left corner, the surrounding counterclockwise-rotating fluid moving downwards progressively deviates horizontally rightwards and briskly turns downwards and leftwards, creating a bend which then arouses deeper inside the bend a tiny, loose clockwise-rotating eddy. Afterwards, this merges with the tiny clockwise-rotating eddy exactly at the bottom left corner, and then the amalgam merges rightwards with the widespread clockwise-rotating leading eddy, detaching it from the bottom wall. Yet, as it raises further upwards, the remnant before suddenly surfaces within it and soon merges rightwards with the widespread clockwise-rotating leading eddy.

Second, a bend at the border of dissimilarly rotating eddies at the bottom right corner (see Fig. 6). A small counterclockwise-rotating eddy stands out at the bottom right corner, arousing exactly at the bottom right corner a tiny clockwise-rotating eddy. A tiny counterclockwise-rotating eddy arouses attached to the right wall a little bit above the bottom right corner, grows, glides downwards attached to the right wall, and merges with the small counterclockwise-rotating eddy at the bottom right

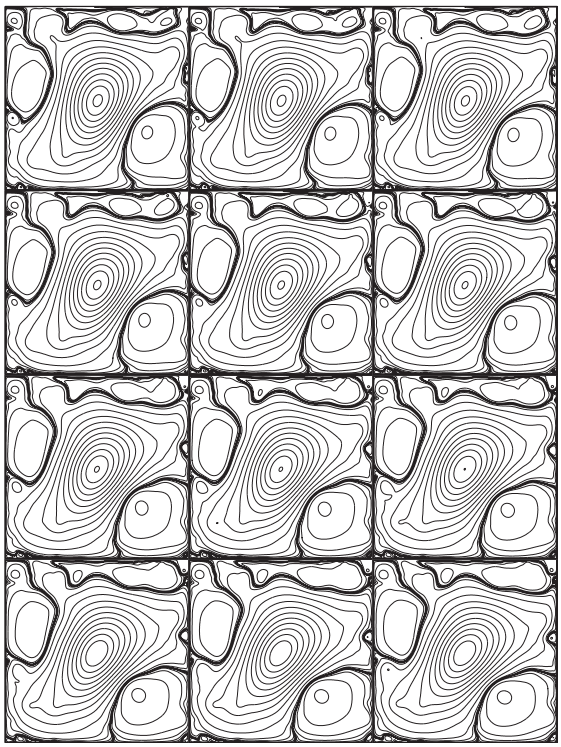

Figure 6: A Third principle's occurrence at the bottom right corner. $\mathrm{Re}=10^6$.

corner, forming out a small counterclockwise-rotating amalgam at the bottom right corner. A wide counterclockwise-rotating eddy looping clockwise reaches the bottom right corner and merges with the amalgam, forming out a wide counterclockwise-rotating amalgam looping clockwise. Reaching the tiny clockwise-rotating eddy exactly at the bottom right corner, the surrounding counterclockwise-rotating fluid moving obliquely upwards deviates slightly further upwards and then turns slightly downwards, creating a bend which slowly loops counterclockwise. The globally counterclockwise-rotating fluid inside the bend whirls locally clockwise and then merges with the globally counterclockwise-rotating fluid at the bend, creating a sharper bend which then arouses deeper inside the bend a tiny, loose clockwise-rotating eddy. Shortly after, this merges with the tiny clockwise-rotating eddy exactly at the bottom right corner. As the wide counterclockwise-rotating amalgam looping clockwise leaves the bottom right corner, the small clockwise-rotating amalgam stands out for a while at the bottom right corner.

Third, a bend between two counterclockwise-rotating eddies at the right wall's lower half (see Fig. 7). A wide clockwise-rotating eddy occupying nearly one-fourth of the square cavity stands out attached to the moving (lid) top wall towards the top right corner, surrounded by a widespread counterclockwise-rotating eddy. A small one stands out attached to the bottom wall towards the bottom right corner. Both merge towards

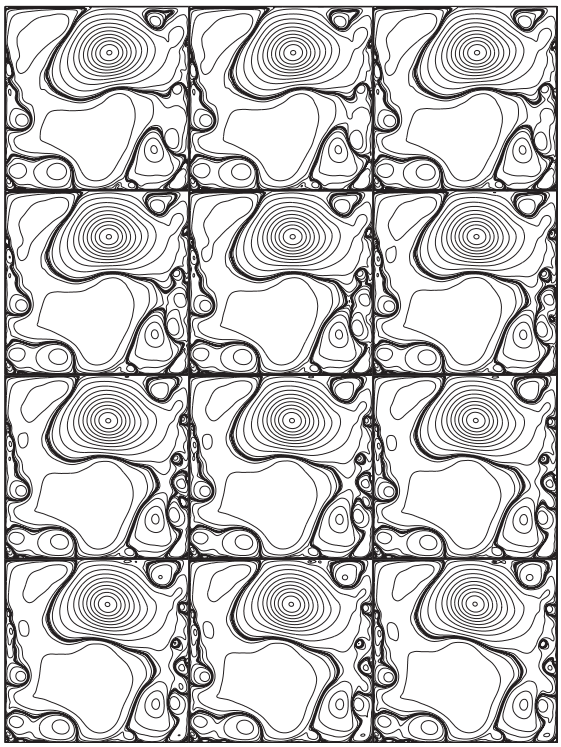

Figure 7: A Third principle's occurrence at the right wall's lower half. $\mathrm{Re}=10^6$.

the right wall's mid-height. From there to the bottom wall, a wide counterclockwise-rotating strip stands out attached to the right wall. A drop detaches from the strip's upside. Within the strip just below the drop, vertically, two small counterclockwise-rotating eddies form out. Between them, on their far side towards the right wall, the one below makes the fluid nearby to turn leftwards; yet, the one above makes it to turn rightwards, creating a bend between them which arouses deeper inside the bend a tiny, loose clockwise-rotating eddy. Shortly after, this attaches to the right wall and then merges leftwards with the surrounding widespread clockwise-rotating eddy. Attached to the right wall, the one above detaches from the strip.

Fourth, a bend between several clockwise-rotating eddies at the top left corner (see Fig. 8). Several small clockwise-rotating eddies merge towards the top left corner, forming out a wide clockwise-rotating amalgam which stands out for a while attached to the left wall a little bit below the top left corner. Several small clockwise-rotating eddies form out within the amalgam. On its right side forms out a long one with two small ones surfacing vertically within. The one above is weak; the one below, strong. On its left side form out vertically two small clockwise-rotating eddies equally strong but weaker than the stronger one and stronger than weaker one on its right side. Towards the center of the amalgam: on its right side, the strong clockwise-rotating eddy below makes the fluid

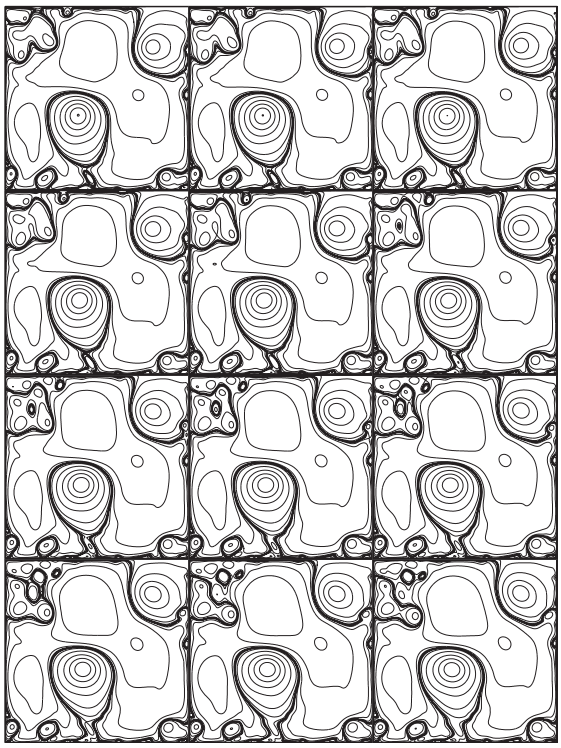

Figure 8: A Third principle's occurrence at the top left corner. $\mathrm{Re}=10^6$.

nearby to turn upwards, but then its influence withers, and the one above, tame, do not sway it anywhere; on its left side, meanwhile, the small clockwise-rotating eddy above makes it to turn leftwards, and the one below, to turn downwards, creating a bend which arouses deeper inside the bend a tiny, loose counterclockwise-rotating eddy. Shortly after, this merges upwards and then rightwards with the surrounding counterclockwise-rotating fluid, detaching a drop from the amalgam. Finally, the amalgam burst out altogether.

And fifth, a bend in the wake of a counterclockwise-rotating eddy looping clockwise at the top right corner (see Fig. 9). A wide clockwise-rotating eddy looping counterclockwise attached to the right wall glides towards the top right corner and merges at the top right corner with a small clockwise-rotating eddy standing out attached to the moving (lid) top wall at the top right corner, looping clockwise around this. Within the amalgam, between both, near to the moving (lid) top wall, a small clockwise-rotating eddy surfaces and arouses closely rightwards, within itself, near attached to the moving (lid) top wall, a tiny, loose counterclockwise-rotating eddy. (This is an occurrence of the Fourth principle.) To the left of it, the former detaches near to the moving (lid) top wall a small counterclockwise-rotating drop from the surrounding widespread counterclockwise-rotating leading eddy which progressively merges with it and then

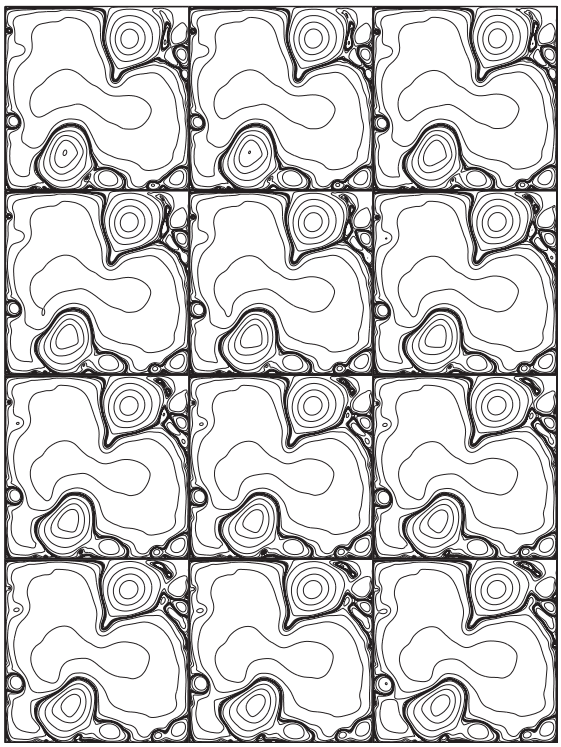

Figure 9: A Third principle's occurrence at the top right corner. $\mathrm{Re}=10^6$.

swings rightwards suspended of it. Shortly after, the amalgam loops clockwise around the former, in the wake of which forms out a bend which arouses deeper inside the bend a tiny, loose counterclockwise-rotating eddy. Afterwards, the amalgam splits out owing to the influence to its right of another clockwise-rotating eddy attached to the right wall a little bit below the top right corner, leaving behind a drop which merges behind with the tiny, loose counterclockwise rotating eddy. The amalgam's remnant merges below with the surrounding widespread counterclockwise-rotating leading eddy.

In the second place, a strong, still clockwise-rotating eddy attached to the moving (lid) top wall may occur anywhere along it, providing occurrences of the Fourth principle. Two instances display below.

First, a small clockwise-rotating eddy's turning away from the moving (lid) top wall at the top left corner (see Fig. 10). A small clockwise-rotating eddy stands out attached to the moving (lid) top wall at the top left corner, surrounded for the most part by a wide counterclockwise-rotating eddy. It turns away from the left wall a little bit below the top left corner, arousing nearby a tiny counterclockwise-rotating eddy attached to the left wall. The interaction of the surrounding globally clockwise-rotating fluid with itself detaches a drop from this which moves horizontally rightwards. Meanwhile, it turns away from the moving (lid) top wall a little bit to the right of the top left corner, arousing

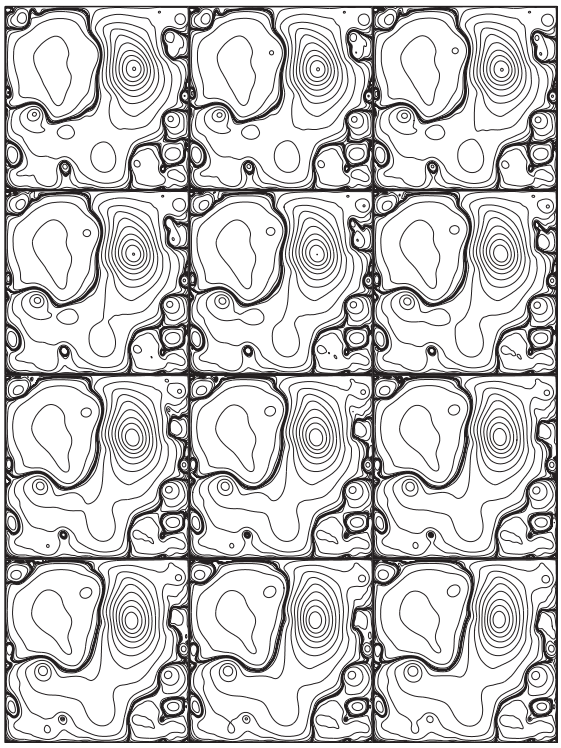

Figure 10: A Fourth principle's occurrence at the top left corner. $\mathrm{Re}=10^6$.

closely rightwards, within itself, near attached to the moving (lid) top wall, a tiny, loose counterclockwise-rotating eddy. It makes this to merge rightwards with the surrounding wide counterclockwise-rotating eddy, the drop before to merge with this, and then the tiny counterclockwise-rotating eddy attached to the left wall a little bit below the top right corner, growing horizontally rightwards, to merge with the drop. It detaches from the moving (lid) top wall. Yet, a drop near to fall from the moving (lid) top wall at the top left corner catches it up. The amalgam sticks to the moving (lid) top wall for a while, but then it detaches from the amalgam and, attached to the left wall, glides further downwards.

Second, a widespread clockwise-rotating eddy's turning away from the moving (lid top wall at the top right corner (see Fig. 11). A widespread clockwise-rotating eddy occupying nearly one-fourth of the square cavity stands out attached to the moving (lid) top wall at the top right corner. Thrice successively, it turns away from the moving (lid) top wall progressively leftwards a little bit to the left of the top right corner, arousing closely rightwards, within itself, near attached to but progressively approaching the top (lid) moving wall, a tiny, loose counterclockwise-rotating eddy which quickly grows and loops clockwise around it. The first one arouses a little bit below the moving (lid) top wall, close to the right wall. Shortly after, the second one arouses and merges with the

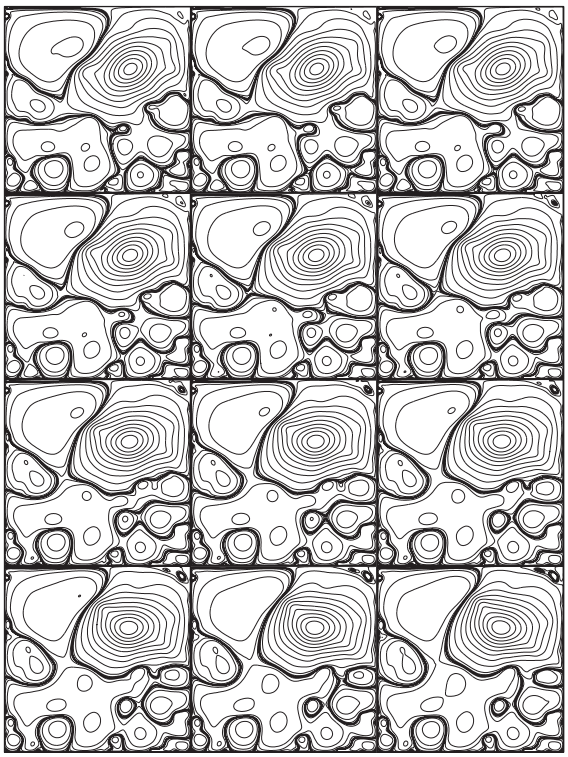

Figure 11: A Fourth principle's occurrence at the top right corner. $\mathrm{Re}=10^6$.

former. But the amalgam soon vanishes. And then, the third one arouses and merges with the amalgam which suddenly surfaces. Yet, a tiny, loose counterclockwise-rotating eddy arouses further leftwards and closer to the moving (lid) top wall, quickly grows, loops clockwise around it, and merges with the amalgam which soon merges with a tiny counterclockwise-rotating eddy arousing attached to the right wall a little bit below the top right corner. Finally, the amalgam, attached to the right wall, glides further downwards.

2.2 The cases $\mathbf{Re}=\mathbf{10^8}$, $\mathbf{5\cdot 10^8}$, $\mathbf{10^9}$

At $\mathrm{Re}=10^8$, $5\cdot 10^8$, 10^9, for fluid starting from data and from rest, from $t=0$ to $t_\infty=50{,}000$, the kinetic energy's behavior resembles somewhat the corresponding one at $\mathrm{Re}=10^6$ (see Figs. 4 and 12). As the Reynolds number $\mathrm{Re}\to\infty$, the upper fragment and the lower fragment distance and then close: the tall high spikes enlarge and then disappear — while the lower fragment stays essentially the same. As the time $t\to\infty$ (at the Reynolds number Re fixed) for fluid starting from data, from $t=0$ to $t_\infty=128{,}125$, they recur from time to time with roughly the same amplitude (see Fig. 13), a DNS involving a total of 32,800,000 temporal iterations.

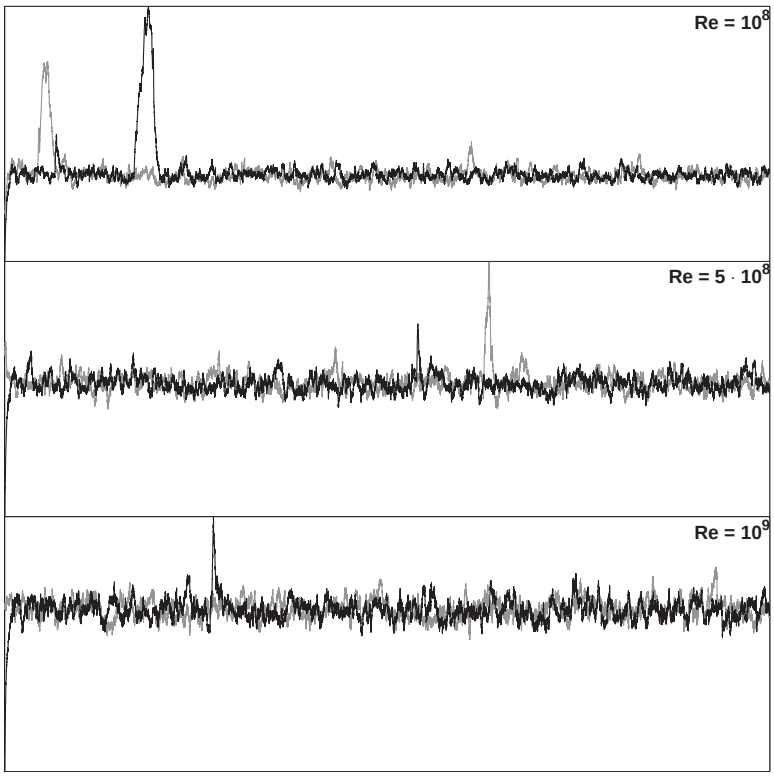

Figure 12: Kinetic energy from $t=0$ to $t_\infty=50{,}000$.

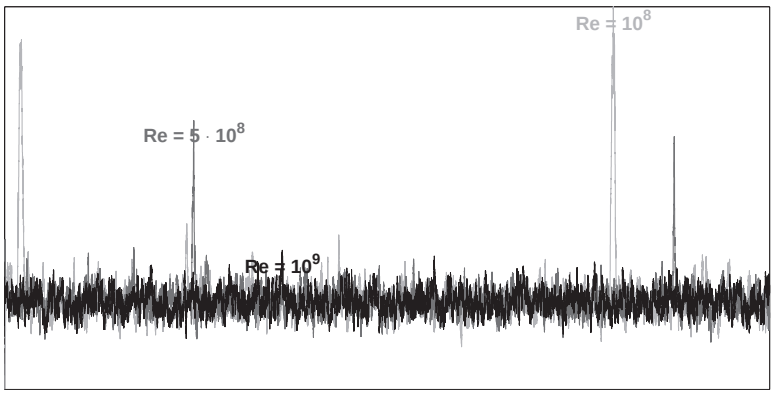

Figure 13: Kinetic energy from $t=0$ to $t_\infty=128{,}125$.

At $\mathrm{Re}=10^8$ let us see an occurrence of the Fourth principle.

A small clockwise-rotating eddy's turning away from the moving (lid) top wall at the top right corner (see Fig. 14). A small clockwise-rotating eddy stands out attached to the moving (lid) top wall at the top right corner, surrounded by a widespread counterclockwise-rotating leading eddy. It turns away from the moving (lid) top wall a

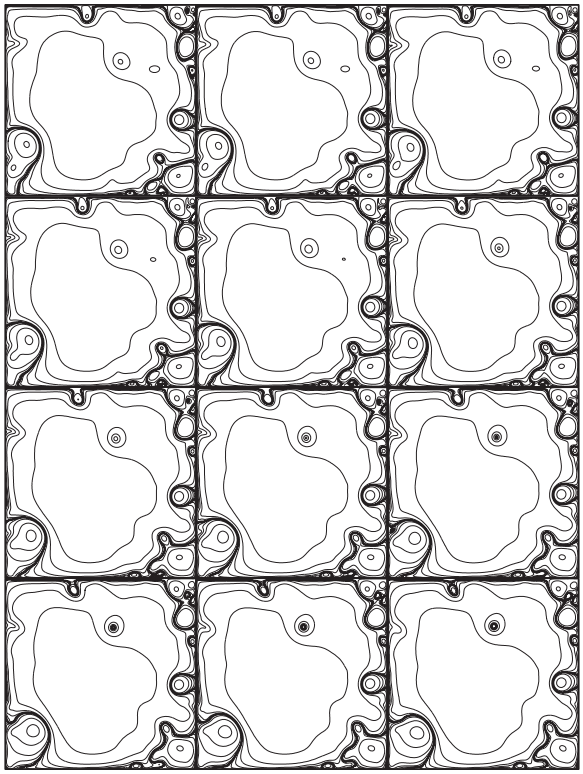

Figure 14: A Fourth principle's occurrence at the top right corner. $\mathrm{Re}=10^8$.

little bit to the left of the top right corner, arousing closely rightwards, within itself, near attached to the moving (lid) top wall, a tiny, loose counterclockwise-rotating eddy which altogether whirls and then — dwindling — loops clockwise around it. Its remnant soon vanishes but then surfaces and again loops clockwise around it, merging below with the widespread counterclockwise-rotating leading eddy.

Next, at $\mathrm{Re}=5\cdot10^8$ let us see how the kinetic energy's fluctuations relate to the leading eddy's switching direction of rotation.

The kinetic energy increasing towards a tall high spike at the upper fragment, a strong eddy occupying more than one-half of the square cavity, stretching out from the left wall to the right wall and from most of the bottom wall to past all the square cavity's mid-height, the leading eddy, rotates clockwise. Upwards stands out a wide counterclockwise-rotating eddy, stretching out from the left wall to the right wall just below a slender clockwise-rotating strip attached to the moving (lid) top wall, which keeps merging and splitting. Other counterclockwise-rotating eddies add to it downwards and leftwards, forming out a widespread counterclockwise-rotating amalgam stretching out from the bottom wall's left side to sharply near the moving (lid) top wall's left side and from there to the right wall's upside. Just before the kinetic energy reaches the top of

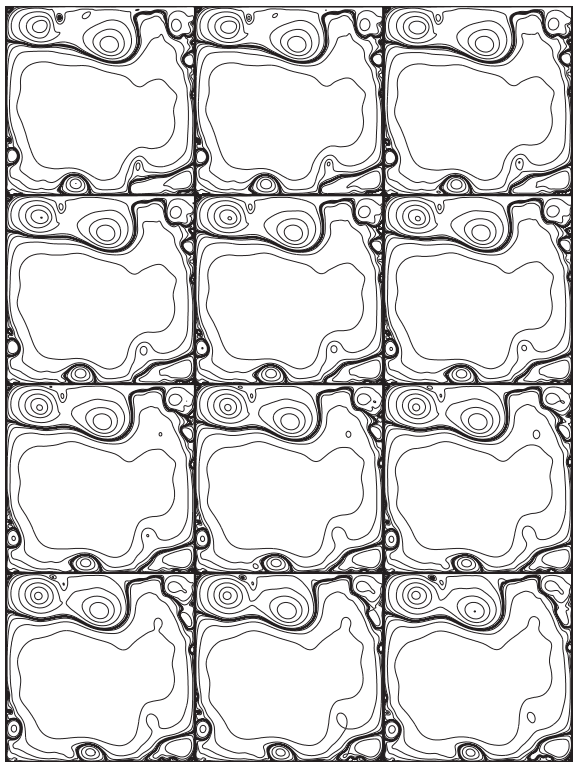

Figure 15: A Fourth principle's occurrence at the moving (lid) top wall's left side. $\mathrm{Re}=5\cdot10^8$.

the tall high spike, it splits out downwards and leftwards, and when the kinetic energy has just past the top of the tall high spike, another counterclockwise-rotating eddy adds to it downwards and leftwards. And then — for an instant — it becomes the leading eddy. For soon it splits upwards and rightwards and again downwards and leftwards, and again a widespread clockwise-rotating eddy, strong, attached to the moving (lid) top wall whose center displaces upwards and rightwards becomes the leading eddy. After a while, it spreads out and attaches somewhat to each rigid wall, surrounding this downwards and leftwards. For a while, it merges and splits. But then it keeps together. Further, the widespread clockwise-rotating leading eddy weakens, and the moving (lid) top wall displaces this rightwards. Consequently, it widens further and thereafter becomes the leading eddy — the kinetic energy diminishing.

At $\mathrm{Re}=5\cdot10^8$ let us see an occurrence of the Fourth principle.

A clockwise-rotating strip's turning away from the moving (lid) top wall at the moving (lid) top wall's left side (see Fig. 15). A widespread clockwise-rotating eddy, a strip attached to the moving (lid) top wall, stretches out from the left wall to past the center of the moving (lid) top wall with, horizontally, two clockwise-rotating eddies surfacing within. Priory, the one on the left forms out by the merging of two clockwise-rotating eddies: a wide clockwise-rotating drop near to fall from the moving (lid) top wall at the

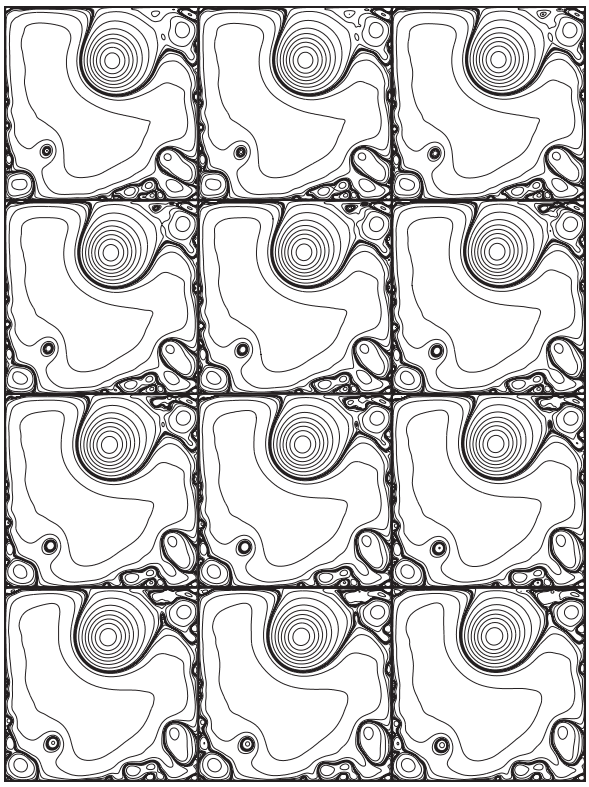

Figure 16: A Third principle's occurrence at the top right corner. $\mathrm{Re}=10^9$.

top left corner and a wide clockwise-rotating eddy looping counterclockwise attached to the moving (lid) top wall gliding towards the top left corner. Suddenly, the globally clockwise-rotating fluid between both, near to the moving (lid) top wall, whirls locally counterclockwise, without arousing deeper inside any tiny, loose counterclockwise-rotating eddy, a whirling which dwindles as both merge but which strengthens when the merging is near completion, arousing deeper inside it a tiny, loose counterclockwise-rotating eddy which grows but dwindles while looping softly around the clockwise-rotating amalgam — the surfacing clockwise-rotating eddy on the left of the strip. As both clockwise-rotating eddies surfacing within the strip approach each other, the one on the left, complete, leaves the moving (lid) top wall a little bit to the right of the top left corner, arousing closely rightwards, within itself, near attached to the moving (lid) top wall, a tiny, loose counterclockwise-rotating eddy which grows, loops clockwise around it, and catches up the former whose remnant meanwhile has strengthened, forming out an amalgam which then merges rightwards with the widespread counterclockwise-rotating leading eddy.

At $\mathrm{Re}=10^9$ let us see an occurrence of the Third principle.

A bend between two clockwise-rotating eddies at the top right corner (see Fig. 16).

A small clockwise-rotating eddy stands out at the top right corner. A wide clockwise-rotating eddy looping counterclockwise reaches the top right corner. Progressively both merge side by side. And then, between both, the latter makes the globally clockwise-rotating fluid on its right to turn downwards; the former, the one on its left to turn upwards, making the globally clockwise-rotating fluid nearby to whirl locally counterclockwise. As the looping progresses, a bend, which appears fleetingly but then surfaces, embraces the fluid whirling locally counterclockwise, arousing deeper inside the bend a tiny, loose counterclockwise-rotating eddy which successively merges below with the widespread counterclockwise-rotating leading eddy and above with a wide counterclockwise-rotating eddy near to the moving (lid) top wall. Both clockwise-rotating eddies detach: the wide one attached to the moving (lid) top wall glides further leftwards; the small one stands out for a while attached to the right wall a little bit below the top right corner.

At $\mathrm{Re}=10^9$, the leading eddy — at its qualitative temporal limit's pace — appears to rotate solely counterclockwise.

3 Summary

Firstly, at extreme Reynolds numbers two principles add at the genesis of tiny, loose counterclockwise- or clockwise-rotating eddies. One concerns the arousing of them owing to the influence of the clockwise- or counterclockwise currents nearby; the other, the arousing of counterclockwise-rotating eddies near attached to the moving (lid) top wall which moves from left to right. Secondly, unexpectedly, the kinetic energy soon reaches the qualitative temporal limit's pace, fluctuating briskly, randomly inside the total kinetic energy range, fluctuations which concentrate on two distinct fragments: one on its upper side, the upper fragment, the other on its lower side, the lower fragment, switching briskly, randomly from each other; and further on many small fragments arousing randomly within both, switching briskly, randomly from one another. As the Reynolds number $\mathrm{Re}\to\infty$, both distance and then close, and the kinetic energy fluctuates shorter and shorter at the upper fragment and longer and longer at the lower fragment, displaying tall high spikes which enlarge and then disappear. As the time $t\to\infty$ (at the Reynolds number Re fixed) they recur from time to time with roughly the same amplitude. For the most part, at the upper fragment the leading eddy rotates clockwise, and at the lower fragment, in stark contrast, it rotates counterclockwise. At $\mathrm{Re}=10^9$ the leading eddy — at its qualitative temporal limit's pace — appears to rotate solely counterclockwise.

Acknowledgments

This research was supported in part by the National Science Foundation Grants No. DMS-0906440 and No. DMS-1206438.

References

[1] E. Barragy and G. F. Carey. Stream function-vorticity driven cavity solution using p finite elements. Comput. & Fluids, 26(5):453–468, 1997.

[2] C.-H. Bruneau and C. Jouron. An efficient scheme for solving steady incompressible Navier-Stokes equations. J. Comput. Phys., 89(2):389–413, 1990.

[3] C.-H. Bruneau and M. Saad. The 2D lid-driven cavity problem revisited. Comput. & Fluids, 35(3):326–348, 2006.

[4] Z.-H. Chai, B.-C. Shi and L. Zheng. Simulating high Reynolds number flow in two-dimensional lid-driven cavity by multi-relaxation-time lattice Boltzmann method. Chinese Phys., 15(8):1855–1863, 2006.

[5] M. Chen, A. Miranville, and R. Temam. Incremental unknowns in finite differences in three space dimensions. Comput. Appl. Math., 14(3):219–252, 1995.

[6] M. Chen and R. Temam. The incremental unknown method I. Appl. Math. Lett., 4(3):73–76, 1991.

[7] M. Chen and R. Temam. The incremental unknown method II. Appl. Math. Lett., 4(3):77–80, 1991.

[8] M. Chen and R. Temam. Incremental unknowns for solving partial differential equations. Numer. Math., 59(3):255–271, 1991.

[9] M. Chen and R. Temam. Incremental unknowns for convection-diffusion equations. Appl. Numer. Math., 11(5):365–383, 1993.

[10] M. Chen and R. Temam. Incremental unknowns in finite differences: Condition number of the matrix. SIAM J. Matrix Anal. Appl., 14(2):432–455, 1993.

[11] M. Chen and R. Temam. Nonlinear Galerkin method in the finite difference case and wavelet-like incremental unknowns. Numer. Math., 64(3):271–294, 1993.

[12] P. Concus, G. H. Golub, and D. P. O'Leary. A generalized conjugate gradient method for the numerical solution of elliptic partial differential equations. Sparse Matrix Computations. Academic Press, 1976. J. R. Bunch and D. J. Rose (Eds.).

[13] P. Constantin. A few results and open problems regarding incompressible fluids. Notices Amer. Math. Soc., 42(6):658–663, 1995.

[14] J. W. Demmel, S. C. Eisenstat, J. R. Gilbert, X. S. Li, and J. W. H. Liu. A supernodal approach to sparse partial pivoting. SIAM J. Matrix Analysis and Applications, 20(3):720–755, 1999.

[15] H. A. Dijkstra, F. W. Wubs, A. K. Cliffe, E. Doedel, I. F. Dragomirescu, B. Eckhardt, A. Yu. Gelfgat, A. L. Hazel, V. Lucarini, A. G. Salinger, E. T. Phipps, J. Sanchez-Umbria, H. Schuttelaars, L. S. Tuckerman, and U. Thiele. Numerical bifurcation methods and their application to fluid dynamics: analysis beyond simulation. Commun. Comput. Phys., 15:1–45, 2014.

[16] E. Erturk, T. C. Corke, and C. Gökçöl. Numerical solutions of 2-D steady incompressible driven cavity flow at high Reynolds numbers. Internat. J. Numer. Methods Fluids, 48(7):747–774, 2005.

[17] C. Eugene Wayne. Vortices and two-dimensional fluid motion. Notices Amer. Math. Soc., 58(1):10–19, 2011.

[18] M. Frigo and S. G. Johnson. The design and implementation of FFTW3. Proc. IEEE, 93(2):216–231, 2005.

[19] S. Garcia. The matricial framework for the incremental unknowns method. Numer. Funct. Anal. Optim., 14(1 & 2):25–44, 1993.

[20] S. Garcia. Numerical study of the incremental unknowns method. Numer. Methods Partial Differential Equations, 10(1):103–127, 1994.

[21] S. Garcia. Higher-order incremental unknowns, hierarchical basis, and nonlinear dissipative evolutionary equations. Appl. Numer. Math., 19(4):467–494, 1996.
[22] S. Garcia. Algebraic conditioning analysis of the incremental unknowns preconditioner. Appl. Math. Modelling, 22(4–5):351–366, 1998.
[23] S. Garcia. Incremental unknowns for solving the incompressible Navier-Stokes equations. Math. Comput. Simulation, 52(5–6):445–489, 2000.
[24] S. Garcia. Incremental unknowns and graph techniques in three space dimensions. Appl. Numer. Math., 44(3):329–365, 2003.
[25] S. Garcia. The lid-driven square cavity flow: From stationary to time periodic and chaotic. Commun. Comput. Phys., 2(5):900–932, 2007.
[26] S. Garcia. Hopf bifurcations, drops in the lid-driven square cavity flow. Adv. Appl. Math. Mech., 1(4):546–572, 2009.
[27] S. Garcia. Aperiodic, chaotic lid-driven square cavity flows. Math. Comput. Simulation, 81(9):1741–1769, 2011.
[28] S. Garcia and F. Tone. Incremental unknowns and graph techniques with in-depth refinement. Int. J. Numer. Anal. Model., 4(2):143–177, 2007.
[29] U. Ghia, K. N. Ghia, and C. T. Shin. High-Re solutions for incompressible flow using the Navier-Stokes equations and a multigrid method. J. Comput. Phys., 48(3):387–411, 1982.
[30] R. Glowinski. Finite Element Methods for the Numerical Simulation of Incompressible Viscous Flow. Introduction to the Control of the Navier-Stokes Equations, volume 28 of Lectures in Applied Mathematics. American Mathematical Society, 1991.
[31] O. Goyon. High-Reynolds number solutions of Navier-Stokes equations using incremental unknowns. Comput. Methods Appl. Mech. Engrg., 130(3–4):319–335, 1996.
[32] F. H. Harlow and J. E. Welch. Numerical calculation of time-dependent viscous incompressible flow of fluid with free surface. Phys. Fluids, 8(12):2182–2189, 1965.
[33] K. Ito, Z. Li, and Z. Qiao. The sensitivity analysis for the flow past obstacles problem with respect to the Reynolds number. Adv. Appl. Math. Mech., 4:21–35, 2012.
[34] J. Kim and P. Moin. Application of a fractional-step method to incompressible Navier-Stokes equations. J. Comput. Phys., 59(2):308–323, 1985.
[35] M. Li, T. Tang, and B. Fornberg. A compact fourth-order finite difference scheme for the steady incompressible Navier-Stokes equations. Internat. J. Numer. Methods Fluids, 20(10):1137–1151, 1995.
[36] R. K. Mohanty and N. Setia. A new fourth-order compact off-step discretization for the system of 2D nonlinear elliptic partial differential equations. East Asian J. Appl. Math., 2:59–82, 2012.
[37] P. Poullet. Staggered incremental unknowns for solving Stokes and generalized Stokes problems. Appl. Numer. Math., 35(1):23–41, 2000.
[38] V. Sarin and A. Sameh. An efficient iterative method for the generalized Stokes problem. SIAM J. Sci. Comput., 19(1):206–226, 1998.
[39] R. Schreiber and H. B. Keller. Driven cavity flows by efficient numerical techniques. J. Comput. Phys., 49(2):310–333, 1983.
[40] T. V. S. Sekhar, B. H. S. Raju, and Y. V. S. S. Sanyasiraju. Higher-order compact scheme for the incompressible Navier-Stokes equations in spherical geometry. Commun. Comput. Phys., 11:99–113, 2012.
[41] A. Shah, H. Guo, and L. Yuan. A third-order upwind compact scheme on curvilinear meshes for the incompressible Navier-Stokes equations. Commun. Comput. Phys., 5:712–729, 2009.
[42] P. N. Shankar and M. D. Deshpande. Fluid mechanics in the driven cavity. Annu. Rev. Fluid

Mech., 32:93–136, 2000.
[43] S. Singh, S. Krithivasan, I. V. Karlin, S. Succi, and S. Ansumali. Energy conserving lattice Boltzmann models for incompressible flow simulations. Commun. Comput. Phys., 13:603–613, 2013.
[44] A. Smith and D. Silvester. Implicit algorithms and their linearisation for the transient incompressible Navier-Stokes equations. IMA J. Numer. Anal., 17(4):527–545, 1997.
[45] L. Song and Y. Wu. Incremental unknowns in three-dimensional stationary problem. Numer. Algorithms, 46(2):153–171, 2007.
[46] L. Song and Y. Wu. Incremental unknowns method based on the θ-scheme for time-dependent convection-diffusion equations. Math. Comput. Simulation, 79(7):2001–2012, 2009.
[47] P. N. Swarztrauber. The methods of cyclic reduction, Fourier analysis and the FACR algorithm for the discrete solution of Poisson's equation on a rectangle. SIAM Rev., 19(3):490–501, 1977.
[48] R. A. Sweet. Direct methods for the solution of Poisson's equation on a staggered grid. J. Comput. Phys., 12(3):422–428, 1973.
[49] R. Temam. Inertial manifolds and multigrid methods. SIAM J. Math. Anal., 21(1):154–178, 1990.
[50] H. A. van der Vorst. Bi-CGSTAB: a fast and smoothly converging variant of Bi-CG for the solution of nonsymmetric linear systems. SIAM J. Sci. Statist. Comput., 13(2):631–644, 1992.
[51] S. P. Vanka. Block-implicit multigrid solution of Navier-Stokes equations in primitive variables. J. Comput. Phys., 65(1):138–158, 1986.
[52] Y. L. Wu, C. Shu, and H. Ding. Simulation of incompressible viscous flows by local DFD-immersed boundary method. Adv. Appl. Math. Mech., 4:311–324, 2012.